

# A Reliable, Time-Predictable Heterogeneous SoC for AI-Enhanced Mixed-Criticality Edge Applications

Angelo Garofalo <sup>x</sup>, Alessandro Ottaviano <sup>x</sup>, Matteo Perotti <sup>id</sup>, Thomas Benz <sup>id</sup>, Yvan Tortorella <sup>id</sup>, Robert Balas <sup>id</sup>, Michael Rogenmoser <sup>id</sup>, Chi Zhang <sup>id</sup>, Luca Bertaccini <sup>id</sup>, Nils Wistoff <sup>id</sup>, Maicol Ciani <sup>id</sup>, Cyril Koenig <sup>id</sup>, Mattia Sinigaglia <sup>id</sup>, Luca Valente <sup>id</sup>, Paul Scheffler <sup>id</sup>, Manuel Eggimann <sup>id</sup>, Matheus Cavalcante <sup>id</sup>, Francesco Restuccia <sup>id</sup>, Alessandro Biondi <sup>id</sup>, Francesco Conti <sup>id</sup>, Frank K. Gurkaynak <sup>id</sup>, Davide Rossi <sup>id</sup>, Luca Benini <sup>id</sup>

arXiv:2502.18953v1 [cs.AR] 26 Feb 2025

**Abstract**—Next-generation mixed-criticality Systems-on-chip (SoCs) for robotics, automotive, and space must execute mixed-criticality AI-enhanced sensor processing and control workloads, ensuring reliable and time-predictable execution of critical tasks sharing resources with non-critical tasks, while also fitting within a sub-2W power envelope. To tackle these multi-dimensional challenges, in this brief, we present a 16nm, reliable, time-predictable heterogeneous SoC with multiple programmable accelerators. Within a 1.2W power envelope, the SoC integrates software-configurable hardware IPs to ensure predictable access to shared resources, such as the on-chip interconnect and memory system, leading to tight upper bounds on execution times of critical applications. To accelerate mixed-precision mission-critical AI, the SoC integrates a reliable multi-core accelerator achieving 304.9 GOPS peak performance at 1.6 TOPS/W energy efficiency. Non-critical, compute-intensive, floating-point workloads are accelerated by a dual-core vector cluster, achieving 121.8 GFLOPS at 1.1 TFLOPS/W and 106.8 GFLOPS/mm<sup>2</sup>.

**Index Terms**—Heterogeneous mixed-critical SoC, time-predictable SoC, hardware acceleration, fault tolerant hardware.

## I. INTRODUCTION

To meet the growing computational demands of artificial intelligence (AI)-enhanced applications in safety-critical domains like automotive, space, and robotics, near-sensors zonal/on-board controllers [1] must efficiently handle compute-intensive tasks while ensuring reliable, time-predictable execution of time-critical tasks (TCTs) [2]. To optimize latency, performance, efficiency, and area, Systems-on-chip (SoCs) must be designed as heterogeneous mixed criticality systems (MCSs) [3], combining general purpose (GP) processors and domain-specific accelerators (DSAs), within a sub-2W power budget typical of high-end microcontrollers [4].

These multi-faceted requirements pose significant design challenges. For instance, achieving time predictability without major performance overhead is hindered by resource conflicts

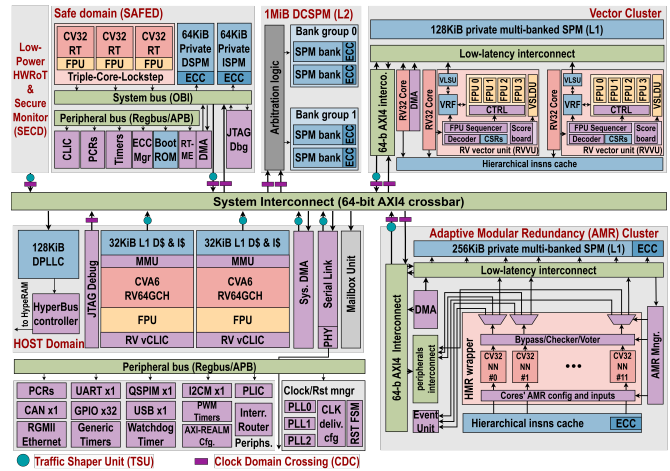


Figure 1. SoC Architecture.

among heterogeneous compute units sharing interconnects and memory endpoints [5], making it difficult to ensure a bounded worst-case execution time (WCET). *Spatial* and *temporal* partitioning of hardware resources [6] are key techniques to mitigate these issues. While recent works partially address this problem in hardware, mainly focusing on interconnects [7], [8], no comprehensive hardware implementation providing observability and controllability of shared resources for predictability has been demonstrated in silicon. As a result, freedom-from-interference or bounded WCET on state-of-the-art (SoA) SoCs [9], [10], [11] is mainly achieved through software mechanisms, leading to significant performance overhead [12].

Another challenge is ensuring that DSAs meet both performance and dependability requirements while remaining compact and low-power. On the one hand, traditional high-precision (floating-point (FP)) tasks for Digital Signal Processing (DSP) (e.g., radar signal processing) and advanced predictive control require acceleration to meet stringent control-loop bandwidth constraints [13], [14]. On the other hand, a new class of AI-intensive low arithmetic precision tasks (e.g. deep neural network inference for object detection, collision avoidance, condition monitoring) require not only tight real-time constraints but also fault tolerance and resiliency [13].

Despite domain-specific acceleration (DSP-control, AI-perception) being crucial for performance and energy efficiency, software programmability remains a fundamental pillar for keeping pace with rapidly evolving algorithms. The extensible nature of the RISC-V (RV) instruction set architecture (ISA)

<sup>x</sup> Both authors contributed equally to this research.  
A. Garofalo, A. Ottaviano, M. Perotti, T. Benz, R. Balas, M. Rogenmoser, C. Zhang, L. Bertaccini, N. Wistoff, C. Koenig, P. Scheffler, M. Eggimann, M. Cavalcante, F. K. Gurkaynak, and L. Benini are with the D-ITET department at ETH Zurich, Switzerland.  
E-mail: {agarofalo,aottaviano}@ethz.ch  
Y. Tortorella, M. Ciani, M. Sinigaglia, L. Valente, F. Conti, D. Rossi are with the Department of Electrical, Electronic, and Information Engineering (DEI), University of Bologna, Italy.  
F. Restuccia is with the Department of Computer Science and Engineering, University of California in San Diego (UCSD), California, USA.  
A. Biondi is with the Department of Excellence in Robotics & AI, Scuola Superiore Sant’Anna, Pisa, Italy.

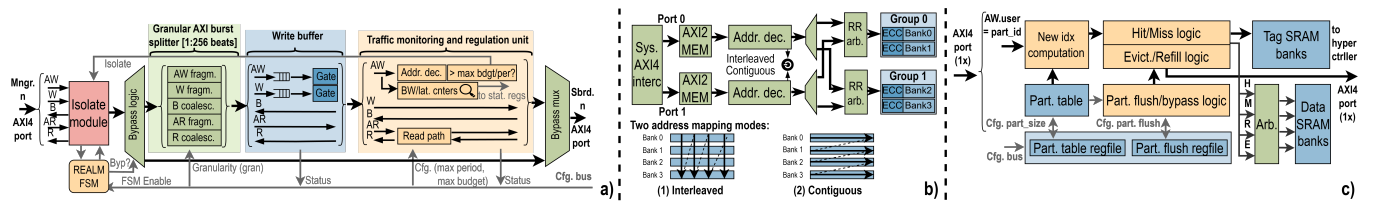


Figure 2. Architectures of the hardware IPs for predictability: a) TSU; b) DCSPM; c) DPLL.

with custom instructions offers a viable approach to specialize instruction processors, striking a balance between efficiency, performance, and programmability [10], [15]. However, while recent research on programmable edge AI processors has mainly focused on performance and efficiency metrics [10], [16], [17], [18], there is a need for silicon-proven, dependable hardware architectures achieving SoA performance and energy efficiency.

To the best of our knowledge, no SoC addresses these challenges holistically. To close this gap, we present a heterogeneous RV SoC implemented in Intel 16nm FinFet technology, featuring three main contributions: **1)** end-to-end time-predictable execution of mixed-criticality tasks (MCTs) enabled by a set of software-programmable hardware IPs for configurable partitioning of shared resources at zero performance overhead, namely: a configurable traffic shaper unit (TSU) for interconnect, a dynamic partitionable last-level cache (DPLL), and the L2 dynamically configurable L2 scratchpad memory (DCSPM); **2)** a 1.07 TFLOPS/W, 107 GFLOPS/mm<sup>2</sup>-at-FP8 dual-core vector floating-point mixed-precision acceleration cluster for FP workloads; **3)** a 1.61 TOPS/W, 260.7 GOPS/mm<sup>2</sup> at 2b 12-core RV integer accelerator cluster with runtime adaptive modular redundancy (AMR) to trade-off performance with reliability in integer mixed-precision mission-critical AI tasks. To enable extensions, benchmarking and comparative analysis, we release the synthesizable hardware description of the SoC design open-source under a liberal license <sup>1</sup>.

## II. SOC ARCHITECTURE

Fig. 1 shows the SoC architecture, operating across three clock domains, each driven by a dedicated PLL. A secure domain (SECD) acts as the SoC’s hardware root of trust (HWRoT), handling the secure boot and crypto services. For hard real-time and safety-critical tasks, the safe domain (SAFED) features a lockstepped triple-RV32-core for reliability, error correction code (ECC)-protected private instruction and data scratchpad memory (SPM) for deterministic memory access, and an enhanced RV core-local interrupt controller (CLIC) with 6-cycle interrupt latency.

Soft real-time tasks with less stringent safety requirements run in the host domain (HOSTD), based on the Cheshire platform [19], extended with a dual-core RV64GCH processor with hardware-assisted virtualization capabilities: it supports concurrent execution of RTOS and GPOS virtual guests (VGs) through RV-compliant H-extension, and virtual interrupts are managed by per-core virtualized CLIC (vCLIC) to reduce interrupt handling and context-switching latency among VGs.

The HOSTD cores have private 32KiB L1 data caches (D\$) and share a 128KiB DPLL, which interfaces with two external HyperRAM chips via a 400Mb/s deterministic access time HyperBUS memory controller. The system interconnect is based on a 64b AXI4 bus. A 1MiB on-chip shared L2 DCSPM is accessible by all domains with 128b/cyc bandwidth. The SoC also includes conventional peripherals, as shown in Fig. 1. Compute-intensive AI/DSP workloads are offloaded to two domain-specific accelerators: the vector and AMR clusters.

**Hardware IPs For Time-Predictability:** MCTs on the SoC can interfere through the interconnect and memory endpoints - L2 DCSPM and HyperRAM accessed via the DPLL, resulting in non-deterministic behavior and significantly increasing execution time of time-critical tasks (TCTs), as detailed in Sec. III.

To ensure predictable communication over AXI4, each initiator is equipped with a software programmable traffic shaper unit (TSU), shown in Fig. 2.a), aimed at reducing execution latency of TCTs in interference scenarios by controlling each initiator’s bandwidth, thereby enforcing a configurable latency upper bound. The TSU comprises three components: **1)** The *granular burst splitter (GBS)* fragments long AXI4 bursts to a configurable size to ensure fair arbitration between asynchronous initiators with burst capabilities running non-critical tasks (NCTs) (e.g., direct memory access (DMA) engines paired with DSAs) and initiators running higher-priority TCTs; **2)** The *write buffer (WB)* buffers AW and W channels, forwarding AW requests and W bursts only when write data is fully within the buffer. This prevents an initiator from holding the W channel, avoiding interconnect stalls; **3)** The *traffic regulation unit (TRU)* assigns each initiator a fixed transfer budget within a configurable communication period.

Favoring TCTs in the interconnect unavoidably affects the performance of NCTs. However, MCTs conflicting on L2 or HyperRAM endpoints can be further isolated by creating interference-free memory paths. DCSPM can be accessed via two AXI4 ports and addressed in contiguous mode to isolate its physical banks. This is configurable at runtime with zero additional latency through aliased memory map addresses, as shown in Fig. 2.b). For NCTs sharing L2 data, the DCSPM operates in interleaved mode to statistically minimize conflicts. For MCTs accessing HyperRAM, the DPLL reduces non-deterministic cache misses by creating set-based spatial partitions of configurable sizes, isolated in hardware and assigned to VGs’ tasks via *part\_id* identifiers linked to AXI4 user signals, as shown in Fig. 2.c). Predictable cache states associated with tasks sharing a partition are maintained by selective partition flushing, preserving the isolation of other partitions.

**Compact, Efficient, RV Vector Cluster:** The proposed SoC integrates a cluster (Fig. 1, top-right) of two compact,

<sup>1</sup><https://github.com/pulp-platform/carfield>

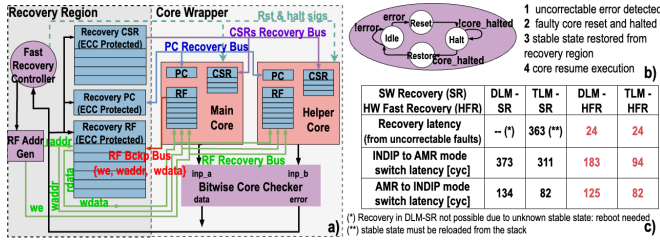


Figure 3. a) Hardware fast recovery (HFR) mechanisms for dual-lockstep mode (DLM) case. b) HFR Finite State Machine. c) AMR performance.

energy-efficient RISC-V Vector Units (RVVUs) controlled by two 32b RV scalar cores, forming a clock-gatable core complex (CC). To minimize access energy on the vector register file (VRF), each RVVU instantiate 2KiB latch-based private VRF, connected to the 16-banks, 1024b/cyc-bandwidth L1 SPM, via four independent 64b vector load-store unit (VLSU) ports and a low-latency interconnect. This allows vector engines to quickly perform unit-strided, non-unit-strided, and indexed memory accesses, improving compute efficiency for both dense and sparse workloads. A third RV core in the cluster manages a 512b/cyc read/write DMA for double-buffered L2-L1 transfers.

Each RVVU is a VLEN=512b RVZve64d processor, supporting formats from FP8 to FP64, bfloat16, integer, and mixed-precision, including sum-of-dot-product (sdotp) operations. Instructions are fetched by the scalar core, decoded by the vector controller to determine the vector length and element width, and executed by the Vector Arithmetic Unit (VAU), achieving a maximum throughput of 256b/cyc for FP operations. The VRF is organized in four banks, each with 3 read and 1 write 256b ports to meet 3x256b/cyc input, 256b/cyc output bandwidth needs of the *vmacc* instruction. The vector cluster achieves 97.9% floating-point unit (FPU) utilization at 15.67 DP-FLOP/cyc on edge-sized matrix multiplications (MatMuls), up to 121.8 FLOP/cyc on FP8xFP8 MatMuls, improving performance by 23.8x to 190.3x over the HOSTD.

**AMR Cluster for Mission-Critical AI:** The adaptive modular redundancy (AMR) cluster, shown in bottom right of Fig. 1, includes 12 RV32IMFC cores sharing a 32-banked 256KiB ECC-protected L1 SPM, accessible through a one-cycle latency interconnect with 921Gb/s (@ 900MHz) bandwidth. A 64b/cyc read, 64b/cyc write DMA enables double-buffered L2-L1 data transfers. Mixed-precision integer DSP/AI tasks are accelerated by the cores through custom RV extensions supporting SIMD sdotp on data formats ranging from 16b to 2b (all possible mixed permutations). A custom *mac-load* instruction increases MAC unit utilization to 94% on MatMuls, overlapping sdotp operations with load instructions.

The RV32 cores can be reconfigured through the AMR hardware to prioritize reliable vs. more performant execution. In the independent mode (INDIP), all 12 cores operate in MIMD for maximum performance. In dual-lockstep mode (DLM) /triple-lockstep mode (TLM) mode, six/four main cores have one/two shadow cores, and instructions are committed after a checker/voting mechanism if no error occurs. The AMR is runtime-programmable; reconfiguration among modes takes 82-183 clock cycles when switching from safety-critical to high-performance sections within application codes (Fig. 3.c)).

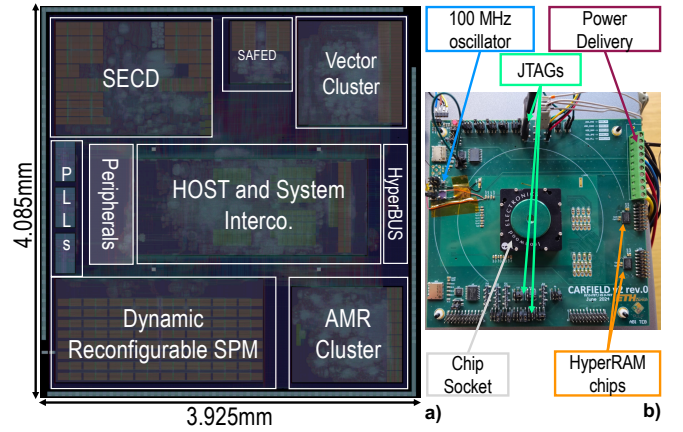
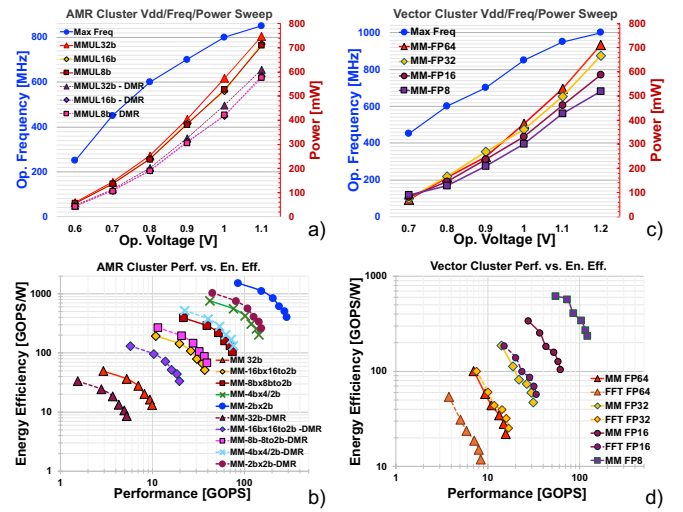


Figure 4. a) SoC micro-graph; b) testing setup.



Accelerators run MatMuls at various precision/configuration at best hw/mem (L1) utilization, at room temp. 25C. 2 OP = 1 MAC

Figure 5. Voltage/Frequency/Power and Performance/Energy Efficiency sweeps of AMR (a, b) and vector (c, d) clusters.

In case of errors, faulty cores are restored to the nearest reliable state in as few as 24 clock cycles thanks to the hardware fast recovery (HFR), shown in Fig. 3.a). The HFR includes ECC-protected recovery registers to back up the internal state of non-faulty cores cycle-by-cycle without extra latency. As shown in Fig. 3.b), DLM with HFR prevents rebooting the cluster upon fault detection, while TLM with HFR is 15x faster than TLM software recovery. When executing in DLM (TLM), the performance penalty is limited to 1.89x (2.85x) compared to INDIP, still achieving 23.1 MAC/cyc (15.3 MAC/cyc) on 8b MatMuls.

### III. EVALUATION AND MEASUREMENTS

Fig. 4 shows the chip micrograph and the standalone printed circuit board (PCB) designed for testing it. The SoC, fabricated with Intel 16nm FinFet technology, operates from 0.6V to 1.1V, with an overall 1.2W power envelope at a nominal 0.8V.

**Performance vs Energy Efficiency:** Fig. 5 evaluates the two clusters, in terms of performance and energy efficiency. Measurements are taken at the maximum operating frequency, sweeping the supply voltage from 0.6V to 1.1V.

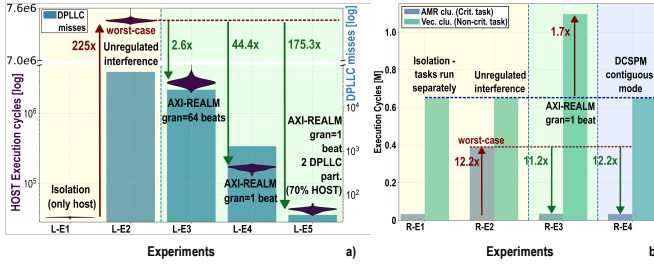


Figure 6. Interference-aware execution of MCTs on the SoC: a) HOSTD runs a TCT accessing HyperRAM, while vector cluster interferes; b) MCTs running on AMR and vector clusters in double-buffering, sharing AXI and DCSPM resources.

The AMR cluster is benchmarked on integer MatMuls, the core kernel of DSP and AI tasks, spanning all supported operands’ precisions, from 32b down to 2b, including mixed-precision formats. The cluster’s cores are configured to run either in INDIP mode for the best performance or in DLM mode for a good trade-off between performance and reliability. The AMR cluster achieves up to 304.9 GOPS on 2b×2b MatMuls (161.4 GOPS in DLM) at 1.1V, 900 MHz, with a peak energy efficiency of 1.6 TOPS/W at 0.6V, 300 MHz (1.1 TOPS/W in DLM). Similarly, we benchmark the vector cluster on FP MatMuls and fast Fourier transforms (FFTs), spanning all supported precisions, reaching a peak performance of 122 GFLOPS on FP8 MatMuls at 1.1V and 1GHz, and a peak energy efficiency of 1.1 TOPS/W at 0.6V and 250 MHz.

**Interference-aware MCTs execution:** Fig. 6 shows how the hardware IPs introduced in Sec. 2 enable interference-aware execution of mixed-criticality tasks (MCTs). In Fig. 6.a) the HOSTD runs a time-critical task (TCT) accessing HyperRAM via the DPLLCC with contiguous stride, while the system DMA interferes by asynchronously transferring data from HyperRAM to the DCSPM with linear bursts. The measurements show the task latency and jitter, as well as the DPLLCC misses generated by the eviction of cache lines among interfering tasks. In unregulated interference, the TCT latency degrades by 225× compared to the isolated (no interference) case (i.e. no interfering DMA). Tuning the *granular burst splitter* and the *traffic regulation unit* of the traffic shaper unit (TSU) in software, we regulate the traffic on the interconnect, reducing the latency by 44.4× compared to the unregulated case. The TSU incurs an additional latency of at most 1 clock cycle due to its write buffer. Moreover, by assigning > 50% spatial partition of the DPLLCC to the TCT, we reduce cache misses, achieving 75% of the isolated (no interference) performance.

In a second scenario, the AMR cluster executes a compute-intensive TCT in reliable mode, and the vector cluster interferes by executing a FP MatMul. Both accelerators move data in double-buffering from L2 to private L1, overlapping data transfer and computation phases. In Fig. 6.b), R-E2, the performance of AMR cluster drops by 12.2× due to conflicts generated by the vector cluster on the interconnect and the DCSPM. Programming the TSU to regulate the traffic in favor of the AMR cluster, we reach 95% of its isolated (no interference) performance (R-E3), degrading the performance of non-critical tasks (NCTs). However, using aliased addresses to access the DCSPM, we create private memory paths (at zero extra performance

SoC	NXP i.MXRT1170 [9]	ST Stellar G / IVLSI23 [11]	ISSCC19 [20]	TCAS-I 24 [10]	This work
Applications	Crossover MCU	Autom. domain controller	Automotive ECU	SoC for nano-drones	SoC for AI-enhanced MCS
Host Cores (ISA) / Safety Cores (ISA)	1xARM Cortex-M7 ARMv8E-M / 1xARM Cortex-M4 ARMv7E-M	6xCortex-R52 (ARMv8-R) (DCLS or in split-lock)	4x Out-of-Order RISC cores (DCLS)	1xCVA6 (RV64GH) / no safety core	2xCVA6 (RV64GH) / 3xCV32RT (RV32IMACF) (TCLS)
Off-chip Memory	HyperRAM/Flash LP5DRAM	2 OctoSPI for HyperRAM/FLASH	n.a.	HyperBUS	HyperBUS iff for HyperRAM/Flash
Safe domain	1x ARM Cortex-M4 (ARMv7E-M)	host acts as safe domain	host acts as safe domain	None	1x CV32RT (triple-lockstep)
AI/ML accelerators	2D graphics unit	ARM NEON extensions	X	1x AI compute cluster	1x Vector cluster / 1x AMR cluster
Max Frequency	M7 @ 1GHz / M4 @ 400 MHz	400 MHz	600 MHz	600 MHz	CVA6 @ 1 GHz / CV32RT @ 1 GHz
Power Envelope	0.978 W @ 1.15 V	1.68 W @ 0.8 V	0.52 W	0.33 W @ 0.8 V	1.2 W @ 0.8 V
Security Features	AES, secure boot	ARM TrustZone	None	None	SecureBoot, AES, KMAC, HMAC
Interrupt Latency	12 clk cycles	20 clk cycles	n.a.	n.a.	6 clock cycles (CV32RT)
HW Virtualization	X	✓	✓ (*)	✓ (RV H ext.) (*)	✓ (RV H ext.) (*) + vCLIC
OSs	RTOS	RTOS	RTOS	RTOS + GPOS	RTOS + GPOS
<b>Time-Predictability Features</b>					
HW Cache partitioning	X	X	X	X	✓
Predict. on-chip comm.	X	✓ (**)	X	X	✓
Dynamic SPM	X	X	X	X	✓

(\*) no hypervisor intervention required to serve interrupts. Direct link to requester Virtual Guest (VG);  
 (\*\*) no specific details reported.

Figure 7. Comparison against SoA heterogeneous SoC for MCS.

overhead) and achieve interference-free execution, matching the isolated (no interference) performance for both tasks (R-E4).

We show that these hardware IPs ensure interference-aware concurrent execution of MCT on shared SoC resources, prioritizing TCTs over NCTs with negligible performance overhead.

#### IV. COMPARISON WITH STATE-OF-THE-ART

**Comparison with Mixed-Criticality SoCs:** Fig. 7 compares the proposed SoC against commercial-off-the-shelf (COTS) and SoA heterogeneous SoC prototypes presented in the literature in the same power class. COTS solutions like the *IMXRT1170* crossover MCUs by NXP [9] mainly address heterogeneous workloads for the average case, relying on ARM Cortex-M cores and GP acceleration units. However, they lack hardware mechanisms for reliability, virtualization, and time predictability, limiting their use as a MCSs. Renesas’ prototype [20] focuses on reliable and virtualized RISC cores, reducing VGs context-switch overheads, but it does not enable resource partitioning among concurrent VGs in hardware, nor does it provide AI/DSP hardware acceleration. Another example is the *Stellar* processor by ST [11]. Despite integrating reliable and real-time ARM Cortex-R52 cores operating in split-lock and an interconnect with Quality of Service mechanisms, it lacks hardware IPs to observe and partition shared memory endpoints. Moreover, it relies solely on GP cores for compute-intensive tasks. In academia, [10] targets AI-enhanced nano-drone applications with a SoC featuring a single-core 64b RV processor and an acceleration cluster similar to ours. However, it lacks features for reliability and time-predictability, limiting the SoC usability in mission-critical scenarios.

At a comparable power envelope, the proposed SoC is the only one that integrates comprehensive hardware mechanisms for time predictability, enabling software-controlled (e.g., via hypervisors) dynamic partitioning of shared resources like interconnects, caches, and SPM. It achieves the fastest interrupt latency response, 2×, 3.3×, and 8.3× lower than [9], [11], and [10], respectively. Additionally, it supports concurrent execution of GPOS and RTOS, integrates a

	TCAS-I 24 [10]	JSSCC23 [18]	JSSCC22 [21]	ISSCC 24 [22]	<b>This Work</b>
Technology	GF 22nm FDSOI	65nm	Intel 16nm FinFet	TSMC 65nm	Intel 16nm FinFet
Type	A	A	B	B	A + B
Die Area	2.2mm <sup>2</sup> (cluster)	4.47 mm <sup>2</sup>	24.1 mm <sup>2</sup>	4 mm <sup>2</sup>	1.14 mm <sup>2</sup> (vector cluster) 1.17 mm <sup>2</sup> (AMR cluster)
Cores	8xRV32IMCCFXflex	10x RV32 + custom ISA ext.	9 x RV64IMAFD + Xwacha4	ARA + DIMC VRF	2 x RVzve64d (vector cluster) 8 x RV32IMCCFXflex (AMR cluster)
Power Range	75 - 200 mW	589 mW	550 mW - 4.1 W (★)	n.a.	29 - 600 mW (vector cluster) 50 - 747 mW (AMR cluster)
Peak SW INT Perf [GOPS]	8x(4x4/2x2b) 26 / 50 / 90	8b 16	n.a.	8b 31.8	8x(8-4-2)/4x(4-2)/2x2b 78.5 / 152.3 / 304.9 41.5 / 80.6 / 161.4 in DLM(★)
Peak SW INT E.E. [GOPS/W]	8x(4x4/2x2b) 540 / 980 / 1800	8b 1800	n.a.	8b 289.1	8x(8-4-2)/4x(4-2)/2x2b 413.6 / 802.6 / 1607 281.4 / 546 / 1093 in DLM (★)
Peak SW INT Area [GOPS/mm <sup>2</sup> ]	8x(4x4/2x2b) 11.8 / 22.7 / 40.9	8b 3.4	n.a.	8b 7.95	8x(8-4-2)/4x(4-2)/2x2b 67.1 / 130.2 / 260.7
Peak FP Perf [GFLOPS]	FP32/FP16(BF16) 4 / 7.9	n.a.	FP64/FP32/FP16 92.1 / 184.2 / 368.4	FP16 (BF16) 25.3	FP64 / 32 / 16 (BF16) / 8 15.7 / 31.3 / 61.5 / 121.8
Peak FP E.E. [GFLOPS/W]	FP32/FP16(BF16) 60 / 120	n.a.	FP64/FP32/FP16 56.5 / 92.3 / 209.5	FP16 (BF16) 230.1	FP64 / 32 / 16 (BF16) / 8 86.9 / 197.8 / 457.8 / 1068.7
Peak FP Area Eff. [GFLOPS/mm <sup>2</sup> ]	FP32/FP16(BF16) 1.8 / 3.6	n.a.	FP64/FP32/FP16 3.98 / 7.9 / 17.9 (★)	FP16 (BF16) 6.3, 34.7 (****)	FP64 / 32 / 16 (BF16) / 8 13.7 / 27.5 / 54 / 106.8

A: programmable edge AI processor; B: vector processor; (★) AMR cluster's cores in DLM (for reliability); (●) derived from info provided in the paper; (\*\*\*\*) scaled to Intel16 tech node.

Figure 8. Comparison against SoA accelerators for FP and edge AI.

HW RoT secure domain with extensive security primitives, and a comprehensive set of programmable accelerators for compute-intensive mixed-criticality workloads, achieving SoA performance and energy efficiency.

**Comparison with edge AI and Vector Processors:** Fig. 8 compares the proposed AMR and vector clusters against SoA vector and edge AI processors. The AMR cluster compares favorably to a similar parallel cluster that supports low-bit-width integer arithmetic but lacks reliability features [10], limiting its use in mission-critical applications. In DLM, it achieves up to 1.8× better performance (3.4× in INDIP) on uniform 8b/4b/2b MatMuls, with 6.4× better area efficiency and comparable energy efficiency. In DLM, it provides 2.6× higher performance than the most efficient 8b integer processor [18], which however lacks support for reliable execution modes. On FP workloads, our vector cluster is the only one that operates over the full range of FP formats, from 64b down to 8b, achieving the highest computing efficiency due to near-ideal resource utilization. Compared to [21], implemented in the same technology node, our cluster demonstrates 2.2× and 3× higher energy and area efficiency, respectively, on FP16 workloads. Additionally, it shows 2.43× better performance, 2×, and 1.6× higher energy and area efficiency than [22], despite the latter leveraging compute-in-memory in the VRF.

## V. CONCLUSION

In this brief, we presented a 16nm reliable, time-predictable heterogeneous RISC-V SoC for AI-enhanced mixed-criticality applications. To the best of our knowledge, this is the first SoC that combines safety features for MCSs with hardware IPs for time-predictable execution of MCTs and leading-edge domain-specialized programmable accelerators within the same heterogeneous SoC. With a peak performance of 304.9 GOPS at 1.6TOPS/W and 260.7 GOPS/mm<sup>2</sup>, and 121.8 GFLOPS at 1.1TFLOPS/W and 107GFLOPS/mm<sup>2</sup>, the proposed SoC offers a comprehensive solution for reliable and deterministic execution of AI/DSP-enhanced mixed critical (MC) edge applications, achieving SoA energy efficiency under 1.2 W power envelope.

## ACKNOWLEDGMENTS

This work was supported by the HORIZON CHIPS-JU TRISTAN (101095947) and ISOLDE (101112274) projects.

## REFERENCES

- [1] O. Burkacky *et al.*, “Getting ready for next-generation E/E architecture with zonal compute.” mckinsey.com/industries/semiconductors/our-insights/getting-ready-for-next-generation-ee-architecture-with-zonal-compute#, Accessed: 12/20/2024.
- [2] F. Rehm *et al.*, “The road towards predictable automotive high-performance platforms,” in *2021 Design, Automation & Test in Europe Conference & Exhibition (DATE)*, pp. 1915–1924, IEEE, 2021.
- [3] Z. Jiang *et al.*, “Re-thinking mixed-criticality architecture for automotive industry,” in *2020 IEEE 38th International Conference on Computer Design (ICCD)*, pp. 510–517, IEEE, 2020.
- [4] M. O. Ojo *et al.*, “A review of low-end, middle-end, and high-end iot devices,” *IEEE Access*, vol. 6, pp. 70528–70554, 2018.
- [5] S. Majumder *et al.*, “Partaa: A real-time multiprocessor for mixed-criticality airborne systems,” *IEEE Transactions on Computers*, vol. 69, no. 8, pp. 1221–1232, 2020.
- [6] T. Kloda *et al.*, “Deterministic memory hierarchy and virtualization for modern multi-core embedded systems,” in *2019 IEEE Real-Time and Embedded Technology and Applications Symposium (RTAS)*, pp. 1–14, IEEE, 2019.
- [7] Z. Jiang *et al.*, “AXI-ic<sup>rt</sup> RT : towards a real-time AXI-interconnect for highly integrated SoCs,” *IEEE Transactions on Computers*, vol. 72, no. 3, pp. 786–799, 2022.
- [8] T. Benz *et al.*, “Axi-realm: Safe, modular and lightweight traffic monitoring and regulation for heterogeneous mixed-criticality systems,” *arXiv preprint arXiv:2501.10161*, 2025.
- [9] N. Semiconductors, “NXP control solutions for industrial automation.” [https://control.com/uploads/articles/NXP\\_CS\\_Industrial\\_TL\\_wp\\_compressed.pdf](https://control.com/uploads/articles/NXP_CS_Industrial_TL_wp_compressed.pdf), 2023. Accessed: 2025-01-03.
- [10] L. Valente *et al.*, “A heterogeneous risc-v based soc for secure nano-uav navigation,” *IEEE Transactions on Circuits and Systems I: Regular Papers*, vol. 71, no. 5, pp. 2266–2279, 2024.
- [11] N. Grossier *et al.*, “Asil-d automotive-grade microcontroller in 28nm fdsoi with full-ota capable 21mb embedded pcm memory and highly scalable power management,” in *2023 IEEE Symposium on VLSI Technology and Circuits (VLSI Technology and Circuits)*, pp. 1–2, IEEE, 2023.
- [12] R. Mancuso *et al.*, “Real-time cache management framework for multi-core architectures,” in *2013 IEEE 19th real-time and embedded technology and applications symp. (RTAS)*, pp. 45–54, 2013.
- [13] R. Islayem *et al.*, “Hardware accelerators for autonomous cars: A review,” *arXiv preprint arXiv:2405.00062*, 2024.
- [14] J. Chung *et al.*, “Hardware accelerators for autonomous vehicles,” in *Artificial Intelligence and Hardware Accelerators*, pp. 269–317, Springer, 2023.
- [15] J. Park *et al.*, “Designing low-power risc-v multicore processors with a shared lightweight floating point unit for iot endnodes,” *IEEE Transactions on Circuits and Systems I: Regular Papers*, vol. 71, no. 9, pp. 4106–4119, 2024.
- [16] K. Xu *et al.*, “An ultra-low power tinyml system for real-time visual processing at edge,” *IEEE Transactions on Circuits and Systems II: Express Briefs*, vol. 70, no. 7, pp. 2640–2644, 2023.
- [17] M. Sun *et al.*, “A 40nm 2tops/w depth-completion neural network accelerator soc with efficient depth engine for realtime lidar systems,” *IEEE Transactions on Circuits and Systems II: Express Briefs*, vol. 70, no. 5, pp. 1704–1708, 2023.
- [18] Y. Ju *et al.*, “A systolic neural cpu processor combining deep learning and general-purpose computing with enhanced data locality and end-to-end performance,” *IEEE Journal of Solid-State Circuits*, vol. 58, no. 1, pp. 216–226, 2022.
- [19] A. Ottaviano *et al.*, “Cheshire: A lightweight, linux-capable risc-v host platform for domain-specific accelerator plug-in,” *IEEE Transactions on Circuits and Systems II: Express Briefs*, vol. 70, no. 10, pp. 3777–3781, 2023.
- [20] S. Otani *et al.*, “2.7 a 28nm 600mhz automotive flash microcontroller with virtualization-assisted processor for next-generation automotive architecture complying with iso26262 asil-d,” in *2019 IEEE International Solid-State Circuits Conference-ISSCC*, pp. 54–56, IEEE, 2019.
- [21] C. Schmidt *et al.*, “An eight-core 1.44-ghz risc-v vector processor in 16-nm finfet,” *IEEE Journal of Solid-State Circuits*, vol. 57, no. 1, pp. 140–152, 2021.
- [22] Y. Wang *et al.*, “30.6 vecim: A 289.13 gops/w risc-v vector co-processor with compute-in-memory vector register file for efficient high-performance computing,” in *2024 IEEE International Solid-State Circuits Conference (ISSCC)*, vol. 67, pp. 492–494, IEEE, 2024.